Treatment of Flue Gas using Graphene Sponge: A Simulation Study

Manish Maurya and Jayant K. Singh*

Department of Chemical Engineering, Indian Institute of Technology, Kanpur, India

ABSTRACT: Grand canonical Monte Carlo simulations are conducted to investigate the adsorption ability of a 3-D graphene sponge (GS) to separate acidic gases from flue gas stream. To assess the adsorption capacity of GS, first, adsorption of pure component flue gas is studied at a temperature of 303 K and varying pressure up to 2.5 bar. Subsequently, the adsorption capacity and selectivity of GS are investigated for a ternary mixture (CO_2/SO_2/N_2) of flue gas under the same conditions. This study shows that the maximum adsorption capacity of GS for pure component flue gas is observed for SO_2 followed by CO_2 and N_2. The adsorption uptake decreases with an increase in pore size of GS. At 1 bar, the amount of adsorption of SO_2 and CO_2 are ~13 mmol/g and ~2.6 mmol/g, respectively. Upon increasing the average pore size to 20 Å, the excess amount decreases by 56% and 58% for SO_2 and CO_2, respectively. The adsorption capacities of GS for CO_2 and SO_2 are better than other carbon-based adsorbents except for CNT bundles. In the case of a ternary mixture of N_2, CO_2, and SO_2 in the mole ratios of 0.8, 0.15, and 0.05, we found that the adsorption behavior follows the same order as in the pure component flue gas adsorption. However, the adsorption amount decreases significantly from that of pure component adsorption amount in GS. The adsorption amount of SO_2 and CO_2 at postcombustion conditions decreases to 1.3 mmol/g and 0.5 mmol/g, respectively, which further decreases upon increasing the average pore size. Selectivity analysis of adsorption shows that the adsorption selectivity of SO_2 over N_2 is the maximum followed by the selectivity of CO_2 over N_2 and SO_2 over CO_2. Both selectivity and uptake capacity decreases with increase in average pore size of GS.
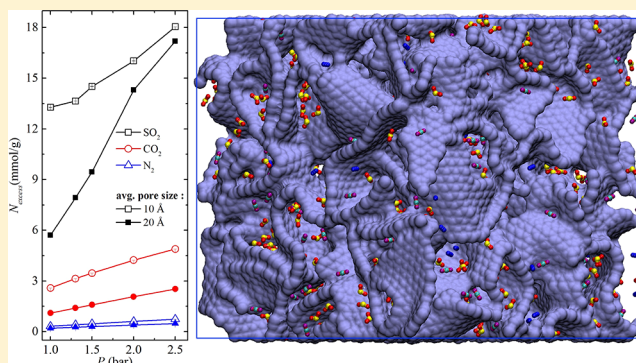
INTRODUCTION

As the world population keeps increasing day by day, energy demand is also growing steadily. More than 85% of this energy demand is fulfilled by burning fossil fuels, which results in the emission of an enormous amount of acidic gases such as CO_2, SO_2, and NO_2, etc.[1] An increase in the concentration of these gases in the environment has led to various environmental and health hazards drawing the significant attention of the world to curtail the emission of these gases. CO_2, the principal greenhouse gas, is considered to be the largest contributor to global warming and climate change. Among all the sources of CO_2 emissions, the power plant industry alone contributes more than 40% to the total CO_2 emissions because coal is the main energy source.[2] Hence, this is the most obvious target for postcombustion capture of CO_2 and SO_2. Carbon capture and storage technology is the most promising solution toward mitigation of CO_2 emission. Other acidic gases such as SO_2 and NO_2 are responsible for acid rain and have a detrimental effect on respiratory systems. The typical concentration of SO_2 in coal-fired flue gas is 700−2500 ppm which makes it very difficult to separate from the mixture of other gases in the flue gas.[3]

Separation of SO_2 from flue gas has received less attention compared to carbon capture technology, and therefore significant research is required to mitigate SO_2 concentration from flue gas stream. Conventionally, flue gas desulfurization is accomplished by an absorption process using different organic and inorganic solvents such as ammonia, limestone, amino acids, and ethylenediamine.[4−8] These conventional methods have some inherent disadvantages like, generation of secondary pollutants, loss of solvents, and excessive energy consumption for regeneration. Therefore, adsorptive separation of these gases from flue gas is an alternate promising solution. Discovering an adsorbent that meets all the criteria is the main challenge in adsorptive separation technology. Thus, for an adsorptive treatment of flue gas, modeling for screening suitable candidates among various choices has become an integral part of the discovery program, before synthesis. Membrane-based gas separation is another approach for flue gas treatment which is growing simultaneously with adsorptive technology. Separation of acidic gases using membrane from flue gas stream is accomplished with the help of selective permeation either through pristine or ionic liquid supported membranes. Carbon molecular sieve, poly(ether sulfone), graphene, and room temperature ionic liquid membranes have been studied extensively to separate CO_2 and SO_2 from flue gas mixture with high selectivity and reversibility.[9−13]
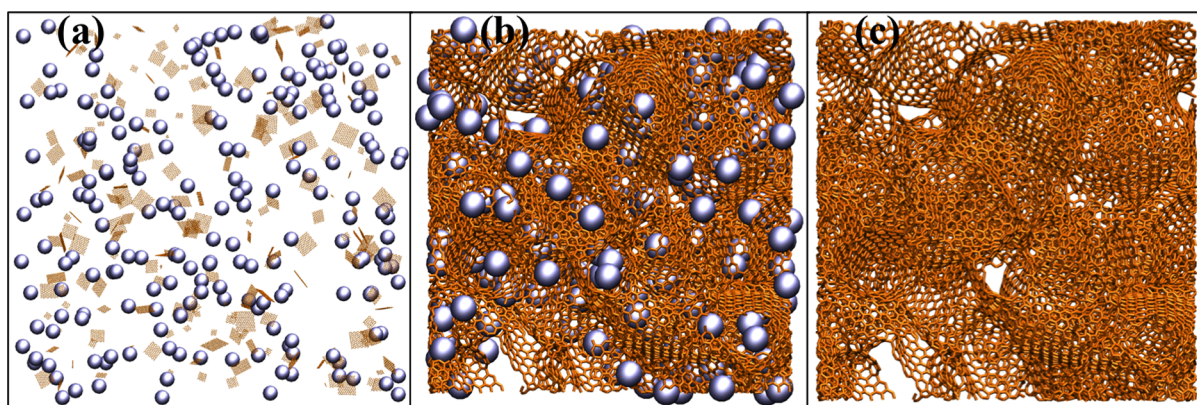
Figure 1. (a) Initial model containing 200 flakes and inclusion particles distributed randomly in simulation box. (b) Composite 3-D structure formed after MD simulations. (c) Porous graphene sponge structure after removing inclusion particles. Silver and orange colors represent inclusion and carbon particles, respectively.

During recent times, many porous materials have been synthesized and modeled to study their capability to capture SO_2 and CO_2 from the flue gas.[14−29] Among these materials, carbon-based adsorbents such as activated carbon, graphene, carbon nanotube, graphite are extensively used and found to be most prominent in gas separation at postcombustion conditions. Apart from carbon materials having well-defined pore size and structures such as activated carbons, covalent organic frameworks, graphene, and carbon nanotubes,[20,22,30] a plethora of amorphous carbon exists in a wide range of density which is equally important for gas separation. For example, Bhatia et al.[31,32] have modeled silicon-carbide derived nanoporous carbon and studied its significance in gas transport for CO_2 and CH_4. In another study, Halder et al.[28] have modeled an experimentally observed porous structure of CMK-5 and studied its applicability in gas separation. They have reported that functionalized CMK-5 models show better gas separation ability compared to various activated carbons. In a recent work, Peng et al.[29] have modeled three different disordered porous carbon materials and found that adsorption selectivities of these materials toward SO_2 and CO_2 in a mixture of flue gas are in line with the ordered porous carbon materials such as carbon nanotubes and graphene nanoribbons. Since amorphous carbon has a very complex structure, it is very difficult to understand its structural property experimentally. In this direction, computer generated models are very helpful in understanding the structural and other thermodynamic properties. There are a wide range of works that exist on modeling amorphous carbon of different densities.[33−37] Modeling porous materials can be classified into three categories:[38] (1) fabrication of structural units of amorphous carbon-based on experimental data; (2) Reverse Monte Carlo method; (3) and a mimetic approach, where the actual experimental method is mimicked by computer simulation using a reactive force field.

In an attempt to understand the mechanical strength of 3-D porous materials that are lighter than air, Qin et al.[39] have modeled a 3-D porous graphene assembly and investigated its mechanical strength. Although many works have been done on the modeling of carbon-based porous structure for gas separation, no work is reported on modeling of 3-D porous material based on graphene flakes. We have seen an opportunity to utilize the mechanically strong 3-D porous graphene material for the purpose of gas separation by tuning its pore size with the help of different inclusion diameters. In

light of the above, in this work, we have used mimetic approach of Qin et al. to model a 3-D porous graphene structure called graphene sponge (GS) using molecular dynamics (MD) simulations, Further, we have performed grand canonical Monte Carlo (GCMC) simulations to assess the ability of GS in adsorptive removal of CO_2 and SO_2 from flue gases.

COMPUTATIONAL METHODS AND POTENTIAL MODELS

Preparation of Graphene Sponge Using Molecular Dynamics Simulations. Atomic models of graphene sponge are obtained by mimicking experimental synthesis of porous materials in classical MD simulations using the LAMMPS software package.[40] In the combined experimental and simulation work of Qin et al., the authors have used a freeze casting method to generate the porous graphene materials.[39] Further, they have developed an MD approach to generate the 3-D model of porous graphene material. We have adopted the cyclic protocol of NVT and NPT ensembles described by Qin et al. to obtain a final equilibrated sponge structure. Initially, 200 graphene flakes with dimensions following log-normal distribution are randomly distributed in simulation box. Initial density of gas phase graphene flakes is 4 mg/cm^3. To mimic the effect of water clusters in freeze casting of porous graphene materials,[41] similar to the approach of Qin et al., 200 spherical inclusion particles are also inserted randomly in simulation box as shown in Figure 1a. In freeze casting of porous materials, the solvent (generally water) is introduced into a dispersed slurry of casting material, and ice crystals are formed by applying a temperature gradient across the material. Once solidification is ended, a freeze-dryer is used to remove ice crystals to obtain the porous material. In this simulation study, the inclusion particle mimics the ice particles to make the structure porous.

Simulations are initiated by fusing and compressing graphene flakes along with inclusion particles in a cyclic manner to get a 3D structure of graphene sponge. One cycle is composed of four stages of alternate NPT-NVT ensembles. The equations of motion are integrated using the velocity-Verlet algorithm with periodic boundary conditions in all directions. AIREBO reactive force field model is used to describe the formation and breaking of carbon bonds in the course of MD simulations.[42] According to this force field, the

interaction energy among pair of carbon atoms is represented as follows:

$$E_{C-C} = \frac{1}{2} \sum_i \sum_{j \neq i} \left[E_{ij}^{REBO} + \sum_{k \neq i} \sum_{l \neq i,j,k} E_{kijl}^{TORSION} \right] \quad (1)$$

where the term REBO in AIREBO potential computes short-range C−C interactions, whereas the term TORSION is an explicit four body potential which describe angle and dihedral potentials. The interaction energy between pair of inclusion atoms and cross interactions between carbon and inclusion atoms are computed using the 12−6 LJ potential model as follows:

$$E_{inc-inc} = E_{C-inc} = \sum_i \sum_{j \neq i} 4\epsilon \left[\left(\frac{\sigma}{r_{ij}} \right)^{12} - \left(\frac{\sigma}{r_{ij}} \right)^6 \right] \quad (2)$$

where $\epsilon = 15$ kcal/mol and $\sigma = 10$ and 20 Å are used to make inclusion atoms stiff with cut off distance of 20 Å. The temperature and pressure are controlled by Nosé−Hoover thermostat in each stage. One complete cycle of four stages is run for 100 ps, i.e., each stage is of 25 ps. In the first stage of cycle, NPT ensemble is used to keep the system at room temperature (300 K) and pressure is increased linearly from 1 to 1000 atm with time step of 0.5 fs. For stage 2, volume is kept constant using NVT ensemble and temperature is increased linearly from 300 to 2000 K in 25 ps. For stage 3, system is relaxed in NVT ensemble for 25 ps. In the final stage, the temperature is reduced back to ambient temperature keeping constant volume in NVT ensemble. After repeating this cycle for more than 15 times, we get the final sponge structure as shown in Figure 1b. Repeating this cycle ensures the convergence of average number of covalent bonds to 1.4 for each carbon atom which is close to that of the actual graphene sheet (1.5 per atom).[39]

After removing inclusion particles, the porous structure as shown in Figure 1c is equilibrated at ambient conditions. This equilibrated structure is further used in GCMC simulations to assess its ability in gas separation from flue gas. Radial distribution of carbon atoms and pore size distributions[43] are shown in Figures 2 and 3, respectively. Radial distribution function of carbon atoms in GS are in agreement with the experimentally observed radial distribution of carbons.[44] The position of the first peak in the radial distribution function of both models is very close to the nearest neighbor distance of 1.42 Å in graphene. The second peak occurs at a distance of 2.52 Å which is the second neighbor distance in six membered
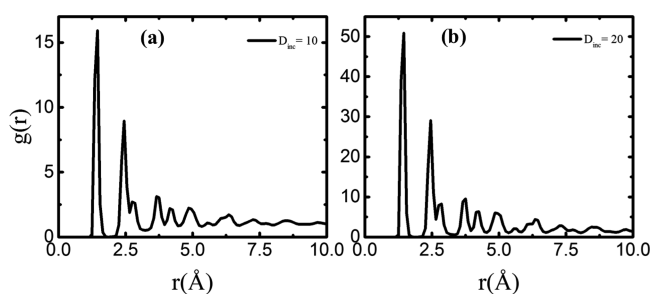
rings with significant contributions from five and seven membered rings. The peak height of radial distribution function in 10 Å average pore size of GS as shown in Figure 2a is less than that of 20 Å average pore size of GS shown in Figure 2b. This indicates that in the case of the large inclusion diameter (20 Å), graphene flakes in the final sponge structure are more correlated and mostly remain intact together. Pore size distribution as shown in Figure 3a suggests that the majority of the pore sizes are around the diameter of inclusion particle. However, a majority of the pore size distribution in the case of the large inclusion diameter, as shown in Figure 3b, is slightly above the inclusion diameter owing to less interlinking among the graphene flakes in the final structure. Using large size inclusion particles results in an open structure and hence it shows a wide range of peaks in pore size distribution. This demonstrates that the size of the water clusters (represented by inclusion particles in this work) in freeze casting of porous materials decides the actual porosity of the surface, as also observed by Qin et al.

Grand Canonical Monte Carlo Simulations. To examine the adsorptive gas separation ability of graphene sponge, Monte Carlo simulations are performed at post-combustion flue gas conditions, i.e., 303 K and pressure is varied up to 2.5 bar. Two different average pore sizes, 10 and 20 Å of GS are studied for gas separation. Flue gas is first modeled as a pure component gas stream of either SO_2, CO_2, or N_2 to examine the more favorable gas component for adsorption. Further, it is modeled as a ternary mixture of SO_2, CO_2, and N_2 in the mole ratio of 5:15:80 to investigate the effect of presence of other components of flue gas stream. Potential model for carbon atoms in GS is taken from Do et al.,[45] and the sponge structure is considered to be frozen during simulation. Gas molecules, SO_2, CO_2, and N_2 are modeled as three site rigid molecules.[46,47] All the potential parameters are listed in Table 1. The interaction energy between two pairs of molecules is expressed as the sum of Lennard−Jones (LJ) and Coulombic interactions as follows:

$$E = \sum_{ij} 4\epsilon_{ij} \left[\left(\frac{\sigma_{ij}}{r_{ij}} \right)^{12} - \left(\frac{\sigma_{ij}}{r_{ij}} \right)^6 \right] + \sum_{ij} \frac{Cq_iq_j}{r_{ij}} \quad (3)$$

where r_{ij} and σ_{ij} are distance between sites i and j of two molecules and the distance at which cross LJ interaction potential is zero, respectively. ϵ_{ij} is the energy parameter between two sites of a molecule, and q_i and q_j are charges on site i and site j of two molecules, respectively. A cutoff distance of 15 Å is used for both LJ and Coulombic interactions. Cross interaction energy parameters are approximated using Lorentz−Berthelot rules and Coulombic interactions are calculated using Ewald summation method. Three Monte Carlo moves are used, viz., displacement, addition/deletion, and rotation with frequencies of 20%, 70%, and 10%, respectively. During the simulation, 5×10^7 MC steps are used for both equilibration and production runs. All the simulations are performed using in-house GCMC code. The code has been used in earlier works to study the adsorption phenomenon in porous materials.[20,28]

Theory of Adsorption. In GCMC simulations, we get the absolute number of adsorbed particles (N_{ad}) in the simulation box. However, in literature, adsorption amount in experimental studies are reported as excess amount of adsorption (N_{excess}). So, to compare the results with the experimental data, absolute
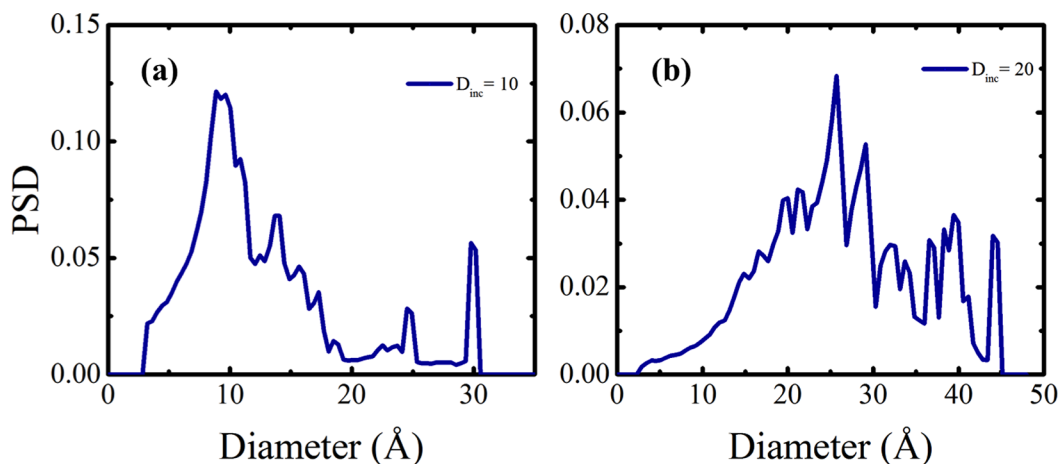

Figure 2. Radial distribution functions between C−C atoms of two structures obtained using two different inclusion diameters (a) $D_{inc} = 10$ Å and (b) $D_{inc} = 20$ Å.

Figure 3. Pore size distribution in graphene sponge obtained using two different inclusion diameters. (a) D_{inc} = 10 Å and (b) D_{inc} = 20 Å.

Table 1. Force Field Parameters for SO$_2$, CO$_2$, N$_2$, and Carbon (C^a) Particles of Adsorbent

atom	σ (Å)	ϵ (kcal/mol)	$q(e)$
S	3.39	0.147	0.59
O	3.05	0.157	−0.295
C	2.80	0.054	0.70
O	3.05	0.157	−0.35
N	3.31	0.072	−0.482
N (COM)	0.0	0.0	0.964
C^a	3.4	0.056	0.0

adsorption amount is converted into excess adsorption by removing the presence of bulk fluid in available space using the following expression:

$$N_{excess} = N_{ad} - \rho_b V_{free} \tag{4}$$

where ρ_b is the bulk density of adsorbate which is obtained from independent GCMC simulation at the same thermodynamic conditions, and V_{free} is the accessible volume for the fluid molecules. Accessible volume can be calculated by several methods reported in the literature.[48−50] In this work, helium adsorption method is used to get free volume.[50] In addition to the excess adsorption data, a thermodynamic quantity of interest is isosteric heat of adsorption, which reflects the amount of heat liberated while adding each molecule in the adsorbed phase. In other words, isosteric heat is a measure of interaction strength between adsorbate and adsorbent molecules which is approximated by the following:[51]

$$q_{st} \approx RT - \left(\frac{\partial U_{ad}}{\partial N_{ad}} \right)_{T,V} \tag{5}$$

where U_{ad} is the total energy of adsorbed phase. The partial derivative in above expression is calculated using fluctuation theory. The resultant expression for isosteric heat of adsorption is shown below:[52]

$$q_{st} = RT - \frac{\langle U_{ad} N_{ad} \rangle - \langle U_{ad} \rangle \langle N_{ad} \rangle}{\langle N_{ad}^2 \rangle - \langle N_{ad} \rangle^2} \tag{6}$$

where the ensemble average is represented by angled brackets.

Adsorption selectivity of surface for species i over species j in a ternary mixture of flue gas is defined as follows:

$$S_{i/j} = \left(\frac{x_i}{x_j} \right) \left(\frac{y_j}{y_i} \right) \tag{7}$$

where x and y are the mole fractions of species in adsorbed and bulk phases, respectively.

■ RESULTS AND DISCUSSION

Adsorption of Pure Component Flue Gas in Graphene Sponge. Figure 4 shows adsorption isotherms of
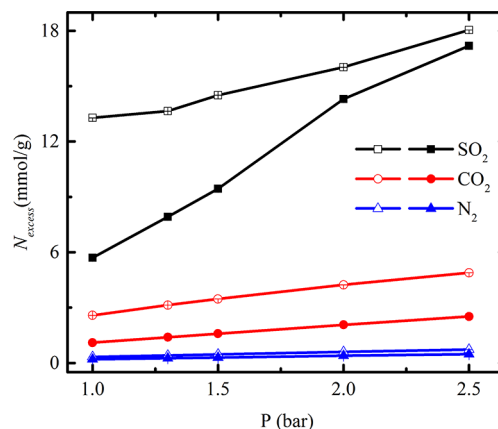

Figure 4. Pure component flue gas adsorption isotherms of SO$_2$ (black), CO$_2$ (red), and N$_2$ (blue) at 303 K. Open symbols are for 10 Å average pore size and filled symbols are for 20 Å average pore size of graphene sponge. Error bar is smaller than the symbol size.

single component flue gases in 10 and 20 Å average pore sizes of GS at 303 K and pressure of 1−2.5 bar. Excess adsorption amounts of SO$_2$ in 10 and 20 Å average pore sizes of GS at 303 K and 2.5 bar are 18.04 mmol/g and 17.2 mmol/g, respectively. Similarly, the adsorption uptake of CO$_2$ in 10 and 20 Å average pore sizes of GS at 303 K and 2.5 bar are 4.88 mmol/g and 2.52 mmol/g, respectively. At a lower pressure, excess adsorption amount of CO$_2$ and SO$_2$ in 20 Å average pore size of GS is significantly less than 10 Å average pore size of GS which is expected due to larger confinement effect in the smaller pore size GS. At a low pressure, say 1 bar, excess adsorption amounts of CO$_2$ in 10 and 20 Å average pore sizes of GS are ∼2.6 mmol/g and ∼1.1 mmol/g, respectively; however, excess adsorption amounts of SO$_2$ in 10 and 20 Å
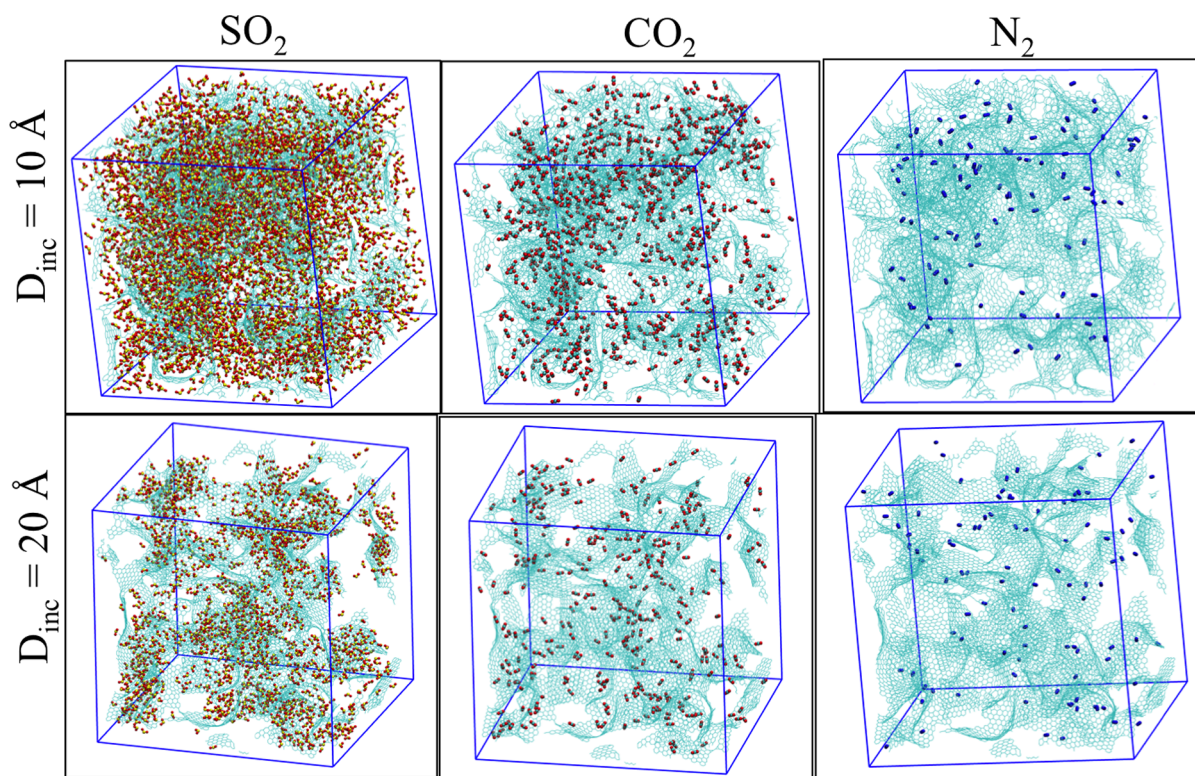
Figure 5. Snapshots of adsorption of SO_2, CO_2, and N_2 at 1 bar and 303 K in two different structures obtained using inclusion particles of diameter 10 Å (top) and 20 Å (bottom), respectively.

average pore sizes of GS are ~13 mmol/g and ~5.7 mmol/g, respectively. The adsorption uptake observed in GS is comparable to CNT based materials. For example, the excess adsorption of SO_2 in bundles of SWCNT and DWCNT at 2.5 bar are ~16 mmol/g and ~16.5 mmol/g, respectively; whereas, excess adsorption of CO_2 in bundles of SWCNT and DWCNT at 2.5 bar are ~7.5 mmol/g and ~7 mmol/g, respectively.[53,54] Adsorption capacity of N_2 is found to be indifferent to the pore size of GS. The excess adsorption capacity of each component increases with increase in pressure. This behavior is seen in both the pore sizes but with increase in average pore size adsorption capacity of each component decreases particularly at low pressure as it can be seen in case of 20 Å average pore size. As far as SO_2 adsorption capacity is concerned, the capacity in 10 Å average pore size GS increases rapidly as compared to 20 Å average pore size GS until the pressure reaches to 1.5 bar. At this pressure, pores of small size GS get saturated with monolayers of SO_2 and after that multilayer starts forming. Beyond this pressure, the rate of adsorption with respect to pressure reduces significantly due to blockage of the pores whereas in large pores, adsorption keeps increasing with pressure. The adsorption capacity of CO_2 and N_2 in both the structures increase linearly with pressure. The adsorption capacity of CO_2 in 10 Å average pore size GS is twice the amount observed in 20 Å average pore size GS until the pores get saturated at a pressure of 2.5 bar. At higher pressures, it is expected that the capacity of 20 Å average pore size GS will be more as its pores will saturate at higher pressures. Adsorption isotherms of nitrogen show that it is weakly adsorbed on GS. The pore size effect on nitrogen adsorption is less in the studied range of pressure. Figure 5 shows the snapshots of the adsorption of pure component flue gas in both the structures. Snapshots of SO_2, CO_2, and N_2 also

corroborate that the adsorption at post-combustion condition is more favorable in smaller pore size GS. The adsorption snapshots also indicate that the confinement effect on SO_2 is more comparable to other flue gas components. SO_2 being the polar molecule shows maximum uptake in GS followed by CO_2 and N_2 at the postcombustion conditions. Gas adsorption shows the following order for both structures: $SO_2 > CO_2 > N_2$.

The energy parameters of fluid molecules play important role in dictating the extent of adsorption in porous materials. We can observe from Figure 6 that those components with higher heats of adsorption have larger uptakes in both structures. Since the isosteric heat of adsorption measures
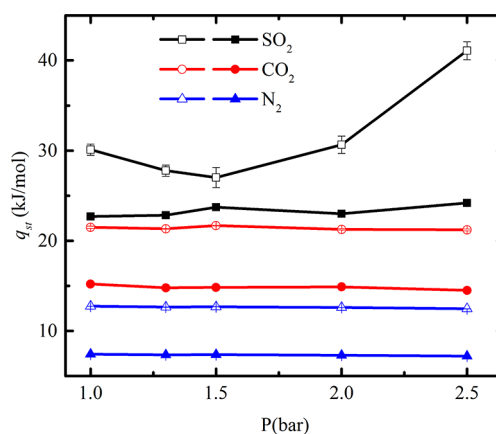

Figure 6. Isosteric heat of adsorption of SO_2 (black), CO_2 (red), and N_2 (blue) at 303 K. Open symbols are for 10 Å average pore size and filled symbols are for 20 Å average pore size of graphene sponge.

the strength of binding with the surface, the maximum adsorption strength is observed for SO_2 in both structures and the least for N_2. At 1 bar, heat of adsorption of SO_2, CO_2, and N_2 are 30, 22, and 13 kJ/mol, respectively. Effect of pressure on heat of adsorption of CO_2 and N_2 is not significant resulting in less contribution of fluid−fluid interactions to the total heat of adsorption. Heat of adsorption of SO_2 first decreases until the saturation of monolayer and then it starts increasing. This can be attributed to multilayer formation of SO_2 in the pore of GS. To understand the heat of adsorption behavior of SO_2, we have plotted the fluid−fluid and fluid−solid interactions in Figure 7. The contribution of fluid−fluid interaction to the
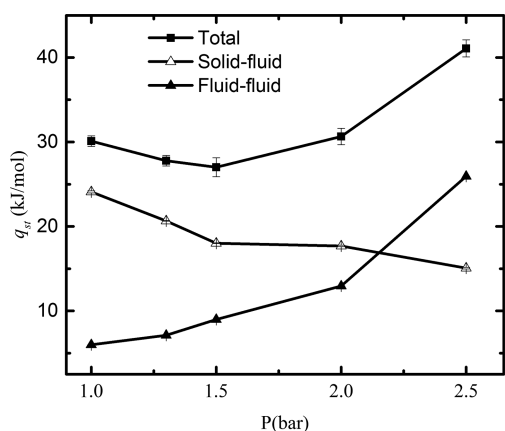

Figure 7. Isosteric heat of adsorption of SO_2 contributed by fluid−fluid, solid−fluid, and total interactions in 10 Å average pore size of graphene sponge at 303 K.

total heat of adsorption increases with increase in adsorption loading of SO_2 compared to fluid−solid interactions which lead to increase in overall heat of adsorption. This behavior is not seen in large pore size GS where pores are not saturated in the studied range of pressure. The heat of adsorption data for CO_2 and N_2 are almost constant with respect to pressure as they have not yet reached the monolayer saturation point. The heat of adsorption decreases with an increase in average pore size, which is also reflected in the reduction of excess adsorption for larger pores. To provide more clarity to the adsorption behavior, we calculated the distribution of adsorbed fluid particles at different pressures. Figure 8a, b shows the absolute density distribution of SO_2 at 1 and 2.5 bar, respectively. The density distribution reveals that at low pressure smaller pore size regions are preferred by gas molecules for adsorption. Subsequently, at a higher pressure gas molecule fill the broader pore size regions. At 1 bar, the distribution of number density is not uniform, and most of the density distribution varies from 0.7 to 0.15 as reflected in the color change from blue to light green. As we increase the pressure above 1.5 bar, multilayer adsorption starts, causing filling of broader pores and enhancement in peaks of the density distribution. At higher pressure, the distribution of number density of SO_2 is in the range from 0.15 to 0.25. Similarly, Figure 8c−f shows the number density distribution of CO_2 and N_2 at two different pressures, respectively. Since the adsorption amount of these gases compared to SO_2 is very low so there are few peaks in the density distribution of CO_2 which is below 0.1 in the blue region on the color scale, and there is no peak in the density profile of N_2 as it is weakly adsorbed. Different peaks in the density distribution are
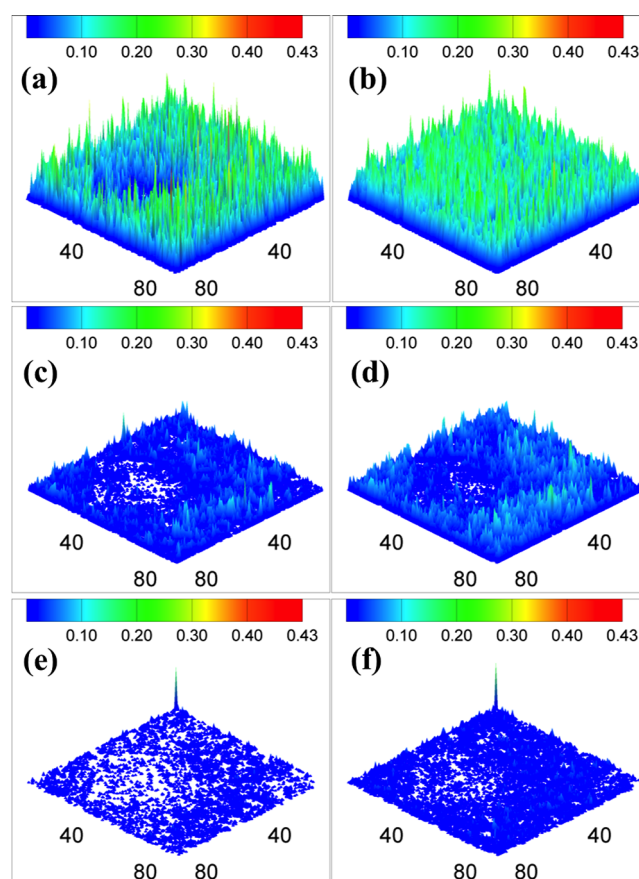

Figure 8. Number density distribution surface of adsorbed SO_2 (a,b), CO_2 (c,d), and N_2 (e,f) at 1 bar (a,c,e) and 2.5 bar (b,d,f) in graphene sponge having average pore size of 10 Å.

because of various pore size distributions throughout the 3-D matrix of carbon atoms. Smaller pores saturate first with increase in the pressure followed by the large pores. The maximum density is observed for SO_2 and the least for N_2 at all pressures.

The usual flue gas emission condition at power plant industry is 1 bar, 303 K. So there is a need to examine adsorption capacity at this condition. At 1 bar, the extent of excess adsorption of SO_2 and CO_2 in GS of 10 Å average pore size are found to be ~13 mmol/g and ~2.6 mmol/g, respectively. Upon increasing average pore size to 20 Å excess amount decreases by 56% and 58% for SO_2 and CO_2, respectively. Recently, many carbon-based materials are extensively used and found to be very useful in gas separation. For example, in a GCMC simulation, Wenjuan et al.[53] have found that an array of single wall carbon nanotube (SWCNT) shows SO_2 adsorption capacity of ~15 mmol/g at 1 bar and 303 K. They have also found that the capacity of array of SWCNT is very sensitive to the pore volume, which is something that we have also observed in GS. In another study, Rahimi et al.[54] have shown that array of double wall carbon nanotube (DWCNT) shows SO_2 adsorption capacity of 14 mmol/g using intertube distance and diameter of 1 and 3 nm, respectively. However, adsorption capacity of CO_2 at 1 bar is found to be 4 mmol/g in DWCNT. In GS, adsorption capacities of SO_2 and CO_2 are less than that obtained in SWCNT and DWCNT because these structures are well ordered and distribution of pore size is uniform throughout the

Table 2. CO$_2$ and SO$_2$ Adsorption Capacities of Some Carbon-Based Adsorbents for Comparison

adsorbent	temperature (K)	pressure (bar)	CO$_2$ (mmol/g)	SO$_2$ (mmol/g)	ref
SWCNT (array)	303	1.0	6.0	15	53
DWCNT (array)	303	1.0	5	13.75	54
graphene nanoribbon	298 (CO$_2$)				
	303 (SO$_2$)	1.0	0.75	8.0	20
activated carbon	323	0.6	0.9	3.3	55
CMK-5	303	1.0	0.8		28
GS	303	1.0	2.5	13	this work

array of SWCNT and DWCNT which results in a high specific surface area. Adsorption capacities of SO$_2$ in most of the activated carbons reported in the literature are found to be less than 6 mmol/g at 1 bar.[55−57] Metal organic framework (MOF), a new class of microporous material, is also extensively studied for gas separation and storage because of its extraordinary specific surface area.[58−62] In a recent study, Xili et al. have synthesized a new MOF and found that its SO$_2$ uptake at atmospheric condition is 11 mmol/g which is the highest among top performing MOFs such as M(bdc)(ted)$_{0.5}$ (9.97 mmol/g),[59] NOTT-300 (Al) (7.1 mmol/g),[62] MFM-300(In) (8.28 mmol/g),[63] and MFM-202a (10.2 mmol/g).[64] Thus, the adsorption capacity of SO$_2$ in GS structure is competing with the existing carbon and metal organic framework materials at postcombustion conditions. Table 2 gives a comparison of adsorption capacities of SO$_2$ and CO$_2$ in different types of adsorbents at low pressure.

Although the effect of temperature is not reported in this work, we expect the adsorption amount of SO$_2$ and CO$_2$ in GS will decrease at elevated temperatures as physisorption is an exothermic process, and according to Le Chatelier principle the amount of adsorption must decrease with an increase in temperature.[65,66] While we have also not considered the effect of water vapor in the current work, it is known that the presence of large size water cluster mainly reduces the adsorption capacity of the carbon materials, however, smaller size clusters may increase its adsorption capacity.[67] Further, to understand the adsorption behavior theoretically, we have fitted the adsorption data with Freundlich and Toth adsorption models,[68]

$$N_{excess} = K_H P^{1/n} \qquad (8)$$

where $1/n$ is a measure of intensity of adsorption and K_H is the Freundlich constant, which is an indicator of adsorption capacity. The Toth isotherm can be presented as follows:[55]

$$q = \frac{q_m bP}{[1 + (bp)^t]^{1/t}} \qquad (9)$$

Where q is the equilibrium adsorption amount corresponds to equilibrium gas pressure P, q_m is the maximum adsorption amount, b is equilibrium adsorption constant, and t measures the surface heterogeneity. The Toth adsorption isotherm reduces to Langmuir isotherm for $t = 1$. We have found that the Freundlich model gives the best fit for all the simulated adsorption data. Tables 3 and 4 summarize the fitted model parameters for both models.

Adsorption of a Ternary Mixture of Flue Gas in Graphene Sponge. Having clear evidence from the previous section of preferred fluid adsorption in GS, now we turn our attention toward adsorption of more realistic flue gas which is a mixture of various gases such as N$_2$, CO$_2$, SO$_2$, and NO$_2$, etc.

Table 3. Freundlich Isotherm Parameters Obtained by Fitting Adsorption Data for Graphene Sponge Having 10 Å Average Pore Size^a

| adsorbate	K_H (mmol/g bar)	$1/n$	R^2
CO$_2$	2.61	1.44	0.99
SO$_2$	12.76	2.81	0.94
N$_2$	0.323	1.12	0.99

^{a}R^2 is the coefficient of determination of fitted data.

Table 4. Toth Isotherm Parameters Obtained by Fitting Adsorption Data for Graphene Sponge Having 10 Å Average Pore Size^a

adsorbate	q_m (mmol/g)	b (bar^{-1})	t	R^2
CO$_2$	24.86	0.16	0.62	0.99
SO$_2$	27.7	1.45	0.72	0.85
N$_2$	8.5	0.04	0.8	0.99

^{a}R^2 is the coefficient of determination of fitted data.

In this section, we have treated flue gas as a mixture of N$_2$, CO$_2$, and SO$_2$ in the mole ratios of 0.8, 0.15, and 0.05, respectively. Figure 9 shows the adsorption isotherms of
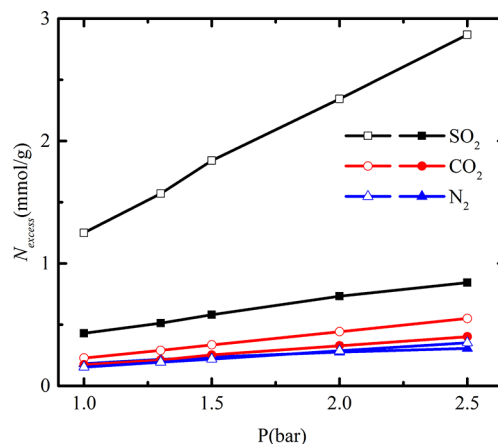
Figure 9. Adsorption isotherms of ternary mixture (SO$_2$/CO$_2$/N$_2$) of flue gas at 303 K. Open symbols are for 10 Å average pore size and filled symbols are for 20 Å average pore size of graphene sponge.

ternary mixture of flue gas. It is obvious from these isotherms that adsorption follows the same order as in the pure component flue gas adsorption. However, the adsorption amount is found to decrease significantly from that of pure component adsorption amount in GS. The adsorption capacity of SO$_2$ and CO$_2$ at postcombustion conditions are 1.3 mmol/g and 0.5 mmol/g, respectively which further decreases on increasing average pore size. This reduction in the uptake capacity of the individual gas molecule is expected as in gas
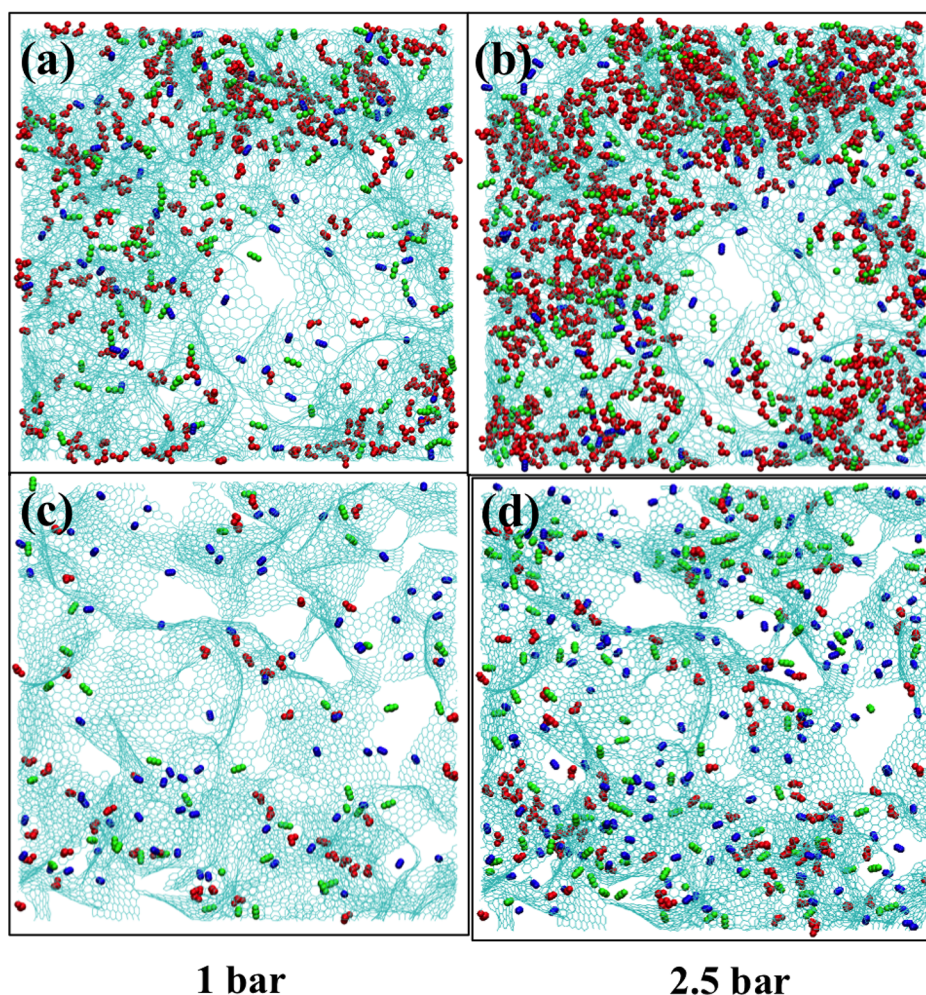
1 bar   2.5 bar

Figure 10. Snapshots of adsorption of ternary mixture ($SO_2/CO_2/N_2$) in two different structures obtained using inclusion particles of diameter 10 Å (top) and 20 Å (bottom). Color coding: Red (SO_2), green (CO_2), and blue (N_2).

mixture molecules which compete with each other to occupy vacant sites of adsorbent. Figure 10 shows the snapshot of mixture adsorption in GS. Snapshot confirms the order of the adsorption amount of different fluid in two structures. This also shows that using the larger pore size GS adsorption amount decreases significantly because of significant vacant space present inside the structure unlike small pore size GS. As the pressure increases, the uptake of fluid molecules increases and this enhancement is more in small average pore size as it is also seen in the case of pure gas adsorption. In the mixture of flue gas, SO_2 is the clear winner in terms of its uptake capacity and strength of adsorption with the surface in competition with other fluid molecules present in the mixture.

To analyze this competitive adsorption of fluid molecules, we have further tested the adsorption selectivity of the fluid mixture in GS. From Figure 11, we can say that the adsorption selectivity of SO_2 over N_2 is at maximum followed by the selectivity of CO_2 over N_2 and SO_2 over CO_2. In our previous study, we had found that adsorption selectivity of ternary mixture follows the same order in functionalized graphene nanoribbons. This order of selectivity is also reported by Rahimi et al. for ternary mixture adsorption in DWCNT. It can be seen that the adsorption selectivity in small average pore size is large compared to larger average pore size. This can be attributed to the confinement effect of carbon atoms around fluid molecules. The effect of confinement is more in case of
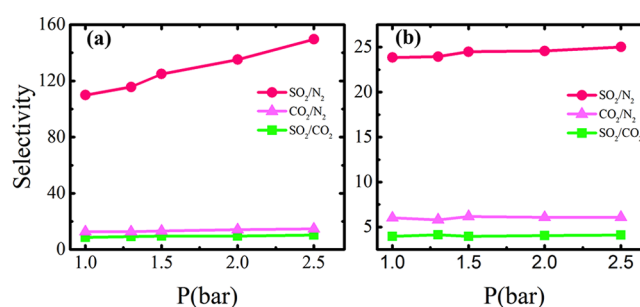

Figure 11. Adsorption selectivity of flue gas mixture in (a) 10 Å average pore size GS and (b) 20 Å average pore size GS, respectively.

SO_2 compared to CO_2 and N_2 as there is a huge difference in vapor pressure of these gases. Due to this selectivity of SO_2 over N_2 increases with pressure in small pore size, whereas it is almost constant with pressure in large pore size as both molecules start competing with each other. The excess adsorption of ternary mixture explains that in larger pore size uptake rate of SO_2 compared to N_2 is not as much as it is in small pore size, causing a reduction in selectivity.

■ **CONCLUSIONS**

In this work, we have generated two 3-D graphene sponge structures having different densities and porosities. Further, we

used GCMC simulations to investigate its adsorption ability for the treatment of flue gas. For this, we have calculated excess adsorption isotherms of different flue gas components at postcombustion conditions. Our simulation results show that the graphene sponge obtained using smaller size inclusion particles have large uptake capacity at postcombustion conditions. As we increase the average pore size of graphene sponge adsorption capacity decreases. We first tested pure component flue gas adsorption capacity in graphene sponge then we moved on for the more realistic ternary mixture ($CO_2/SO_2/N_2$) of flue gas adsorption. Pure component adsorption results show that SO_2 adsorbs preferably over CO_2 and N_2. At 1 bar, the excess adsorption of SO_2 and CO_2 in GS of 10 Å average pore size are found to be ∼13 mmol/g and ∼2.6 mmol/g, respectively. Upon increasing the average pore size to 20 Å, an excess amount decreases by 56% and 58% for SO_2 and CO_2, respectively.

In the case of a ternary mixture, we have treated flue gas as a mixture of N_2, CO_2, and SO_2 in the mole ratios of 0.8, 0.15, and 0.05, respectively. We found that the adsorption amount follows the same order as in the pure component flue gas adsorption, but the adsorption amount decreases significantly from that of pure component adsorption amount in GS. The adsorption capacity of SO_2 and CO_2 at post-combustion conditions are 1.3 mmol/g and 0.5 mmol/g, respectively, which further decreases on increasing pore size. Selectivity analysis of adsorption shows that adsorption selectivity of SO_2 over N_2 is the maximum followed by selectivity of CO_2 over N_2 and SO_2 over CO_2. Thus, our results indicate that graphene sponge obtained using smaller size inclusion particles is a promising material for treatment of flue gas at postcombustion conditions.

■ AUTHOR INFORMATION

Corresponding Author
*E-mail: jayantks@iitk.ac.in (J.K.S.).
ORCID 🔾
Jayant K. Singh: 0000-0001-8056-2115
Notes
The authors declare no competing financial interest.

■ REFERENCES

(1) Rubin, E. S.; Mantripragada, H.; Marks, A.; Versteeg, P.; Kitchin, J. The Outlook for Improved Carbon Capture Technology. *Prog. Energy Combust. Sci.* **2012**, *38*, 630−671.
(2) *Inventory of U.S. Greenhouse Gas Emissions and Sinks*; 1990−2015.
(3) Rao, A. B.; Rubin, E. S. A Technical, Economic, and Environmental Assessment of Amine-Based CO_2 Capture Technology for Power Plant Greenhouse Gas Control. *Environ. Sci. Technol.* **2002**, *36*, 4467−4475.
(4) Tang, Z.-g.; Zhou, C.-c.; Chen, C. Studies on Flue Gas Desulfurization by Chemical Absorption Using an Ethylenediamine-Phosphoric Acid Solution. *Ind. Eng. Chem. Res.* **2004**, *43*, 6714−6722.
(5) He, B.; Zheng, X.; Wen, Y.; Tong, H.; Chen, M.; Chen, C. Temperature Impact on SO_2 Removal Efficiency by Ammonia Gas Scrubbing. *Energy Convers. Manage.* **2003**, *44*, 2175−2188.
(6) Deng, R.; Jia, L.; Song, Q.; Su, S.; Tian, Z. Reversible Absorption of SO_2 by Amino Acid Aqueous Solutions. *J. Hazard. Mater.* **2012**, *229−230*, 398−403.
(7) Stromberg, A.-M.; Karlsson, H. T. Limestone based Spray Dry Scrubbing of SO_2. *Chem. Eng. Sci.* **1988**, *43*, 2095−2102.
(8) van Dam, M. H. H.; Lamine, A. S.; Roizard, D.; Lochon, P.; Roizard, C. Selective Sulfur Dioxide Removal Using Organic Solvents. *Ind. Eng. Chem. Res.* **1997**, *36*, 4628−4637.
(9) Sedigh, M. G.; Xu, L.; Tsotsis, T. T.; Sahimi, M. Transport and Morphological Characteristics of Polyetherimide-Based Carbon Molecular Sieve Membranes. *Ind. Eng. Chem. Res.* **1999**, *38*, 3367−3380.
(10) Sedigh, M. G.; Onstot, W. J.; Xu, L.; Peng, W. L.; Tsotsis, T. T.; Sahimi, M. Experiments and Simulation of Transport and Separation of Gas Mixtures in Carbon Molecular Sieve Membranes. *J. Phys. Chem. A* **1998**, *102*, 8580−8589.
(11) Jiang, Y.-Y.; Zhou, Z.; Jiao, Z.; Li, L.; Wu, Y.-T.; Zhang, Z.-B. SO_2 Gas Separation Using Supported Ionic Liquid Membranes. *J. Phys. Chem. B* **2007**, *111*, 5058−5061.
(12) Rafiq, S.; Man, Z.; Maulud, A.; Muhammad, N.; Maitra, S. Separation of CO_2 from CH_4 using Polysulfone/Polyimide Silica Nanocomposite Membranes. *Sep. Purif. Technol.* **2012**, *90*, 162−172.
(13) Liu, H.; Chen, Z.; Dai, S.; Jiang, D.-e. Selectivity trend of Gas Separation through Nanoporous Graphene. *J. Solid State Chem.* **2015**, *224*, 2−6.
(14) Bagreev, A.; Bashkova, S.; Bandosz, T. J. Adsorption of SO_2 on Activated Carbons: The Effect of Nitrogen Functionality and Pore Sizes. *Langmuir* **2002**, *18*, 1257−1264.
(15) Grzyb, B.; Albiniak, A.; Broniek, E.; Furdin, G.; Mareche, J.; Begin, D. SO_2 Adsorptive Properties of Activated Carbons Prepared from Polyacrylonitrile and its Blends with Coal-tar Pitch. *Microporous Mesoporous Mater.* **2009**, *118*, 163−168.
(16) Lopez, D.; Buitrago, R.; Sepulveda-Escribano, A.; Rodriguez-Reinoso, F.; Mondragon, F. Low Temperature Catalytic Adsorption of SO_2 on Activated Carbon. *J. Phys. Chem. C* **2008**, *112*, 15335−15340.
(17) Srinivasan, A.; Grutzeck, M. W. The Adsorption of SO_2 by Zeolites Synthesized from Fly Ash. *Environ. Sci. Technol.* **1999**, *33*, 1464−1469.
(18) Ivanova, E.; Koumanova, B. Adsorption of Sulfur Dioxide on Natural Clinoptilolite Chemically Modified with Salt Solutions. *J. Hazard. Mater.* **2009**, *167*, 306−312.
(19) Llanos, J. L.; Fertitta, A. E.; Flores, E. S.; Bottani, E. J. SO_2 Physisorption on Exfoliated Graphite. *J. Phys. Chem. B* **2003**, *107*, 8448−8453.
(20) Maurya, M.; Singh, J. K. A grand canonical Monte Carlo Study of SO_2 Capture using Functionalized Bilayer Graphene Nanoribbons. *J. Chem. Phys.* **2017**, *146*, 044704.
(21) Wang, W.; Peng, X.; Cao, D. Capture of Trace Sulfur Gases from Binary Mixtures by Single-Walled Carbon Nanotube Arrays: A Molecular Simulation Study. *Environ. Sci. Technol.* **2011**, *45*, 4832−4838.
(22) Yang, Y.-B.; Rahimi, M.; Singh, J. K.; Bohm, M. C.; Muller-Plathe, F. Adsorption and Condensation of SO_2 in Double-Walled Carbon Nanotube Arrays Studied by Monte Carlo Simulations and Simple Analytical Models. *J. Phys. Chem. C* **2016**, *120*, 7510−7521.
(23) Majumdar, S.; Maurya, M.; Singh, J. K. Adsorptive Separation of CO_2 From Multicomponent Mixtures of Flue Gas in Carbon Nanotube Arrays: A Grand Canonical Monte Carlo Study. *Energy Fuels* **2018**, *32*, 6090−6097.
(24) Song, X.-D.; Wang, S.; Hao, C.; Qiu, J.-S. Investigation of SO_2 Gas Adsorption in Metal-Organic Frameworks by Molecular Simulation. *Inorg. Chem. Commun.* **2014**, *46*, 277−281.
(25) Savage, M.; Cheng, Y.; Easun, T. L.; Eyley, J. E.; Argent, S. P.; Warren, M. R.; Lewis, W.; Murray, C.; Tang, C. C.; Frogley, M. D.; et al. Selective Adsorption of Sulfur Dioxide in a Robust Metal-Organic Framework Material. *Adv. Mater.* **2016**, *28*, 8705−8711.

(26) Mochida, I.; Korai, Y.; Shirahama, M.; Kawano, S.; Hada, T.; Seo, Y.; Yoshikawa, M.; Yasutake, A. Removal of SO$_x$ and NO$_x$ over Activated Carbon Fibers. *Carbon* **2000**, *38*, 227−239.

(27) Bashkova, S.; Bagreev, A.; Locke, D. C.; Bandosz, T. J. Adsorption of SO$_2$ on Sewage Sludge-Derived Materials. *Environ. Sci. Technol.* **2001**, *35*, 3263−3269.

(28) Halder, P.; Maurya, M.; Jain, S. K.; Singh, J. K. Understanding Adsorption of CO$_2$, N$_2$, CH$_4$ and Their Mixtures in Functionalized Carbon Nanopipe Arrays. *Phys. Chem. Chem. Phys.* **2016**, *18*, 14007−14016.

(29) Peng, X.; Jain, S. K.; Singh, J. K. Adsorption and Separation of N$_2$/CH$_4$/CO$_2$/SO$_2$ Gases in Disordered Carbons Obtained Using Hybrid Reverse Monte Carlo Simulations. *J. Phys. Chem. C* **2017**, *121*, 13457−13473.

(30) Olajire, A. A. Recent Advances in The Synthesis of Covalent Organic Frameworks for CO$_2$ Capture. *J. CO$_2$ Utilization* **2017**, *17*, 137−161.

(31) Farmahini, A. H.; Shahtalebi, A.; Jobic, H.; Bhatia, S. K. Influence of Structural Heterogeneity on Diffusion of CH$_4$ and CO$_2$ in Silicon Carbide-Derived Nanoporous Carbon. *J. Phys. Chem. C* **2014**, *118*, 11784−11798.

(32) Bhatia, S. K. Characterizing Structural Complexity in Disordered Carbons: From the Slit Pore to Atomistic Models. *Langmuir* **2017**, *33*, 831−847.

(33) Thomson, K. T.; Gubbins, K. E. Modeling Structural Morphology of Microporous Carbons by Reverse Monte Carlo. *Langmuir* **2000**, *16*, 5761−5773.

(34) Bhatia, S. K. Characterizing Structural Complexity in Disordered Carbons: From the Slit Pore to Atomistic Models. *Langmuir* **2017**, *33*, 831−847.

(35) Jain, S. K.; Pellenq, R. J.-M.; Pikunic, J. P.; Gubbins, K. E. Molecular Modeling of Porous Carbons Using the Hybrid Reverse Monte Carlo Method. *Langmuir* **2006**, *22*, 9942−9948.

(36) de Tomas, C.; Suarez-Martinez, I.; Vallejos-Burgos, F.; Lòpez, M. J.; Kaneko, K.; Marks, N. A. Structural Prediction of Graphitization and Porosity in Carbide-derived Carbons. *Carbon* **2017**, *119*, 1−9.

(37) Farmahini, A. H.; Bhatia, S. K. Hybrid Reverse Monte Carlo Simulation of Amorphous Carbon: Distinguishing between Competing Structures obtained Using Different Modeling Protocols. *Carbon* **2015**, *83*, 53−70.

(38) Ranganathan, R.; Rokkam, S.; Desai, T.; Keblinski, P. Generation of Amorphous Carbon Models using Liquid Quench Method: A Reactive Molecular Dynamics Study. *Carbon* **2017**, *113*, 87−99.

(39) Qin, Z.; Jung, G. S.; Kang, M. J.; Buehler, M. J. The Mechanics and Design of a Lightweight Three-Dimensional Graphene Assembly. *Sci. Adv.* **2017**, *3*, e1601536

(40) Plimpton, S. Fast Parallel Algorithms for Short-Range Molecular Dynamics. *J. Comput. Phys.* **1995**, *117*, 1−19.

(41) Li, W. L.; Lu, K.; Walz, J. Y. Freeze Casting of Porous Materials: Review of Critical Factors in Microstructure Evolution. *Int. Mater. Rev.* **2012**, *57*, 37−60.

(42) Stuart, S. J.; Tutein, A. B.; Harrison, J. A. A Reactive Potential for Hydrocarbons with Intermolecular Interactions. *J. Chem. Phys.* **2000**, *112*, 6472−6486.

(43) Gelb, L. D.; Gubbins, K. E. Pore Size Distributions in Porous Glasses: A Computer Simulation Study. *Langmuir* **1999**, *15*, 305−308.

(44) Beeman, D.; Silverman, J.; Lynds, R.; Anderson, M. R. Modeling Studies of Amorphous Carbon. *Phys. Rev. B: Condens. Matter Mater. Phys.* **1984**, *30*, 870−875.

(45) Do, D. D.; Do, H. D. Evaluation of 1-Site and 5-Site Models of Methane on Its Adsorption on Graphite and in Graphitic Slit Pores. *J. Phys. Chem. B* **2005**, *109*, 19288−19295.

(46) Ketko, M. H.; Kamath, G.; Potoff, J. J. Development of an Optimized Intermolecular Potential for Sulfur Dioxide. *J. Phys. Chem. B* **2011**, *115*, 4949−4954.

(47) Potoff, J. J.; Siepmann, J. I. Vapor-Liquid Equilibria of Mixtures Containing Alkanes, Carbon Dioxide, and Nitrogen. *AIChE J.* **2001**, *47*, 1676−1682.

(48) Mahdizadeh, S. J.; Tayyari, S. F. Influence of Temperature, Pressure, Nanotube's Diameter and Intertube Distance on Methane Adsorption in Homogeneous Armchair Open-Ended SWCNT Triangular Arrays. *Theor. Chem. Acc.* **2011**, *128*, 231−240.

(49) Do, D. D.; Do, H. D. Modeling of Adsorption on Nongraphitized Carbon Surface: GCMC Simulation Studies and Comparison with Experimental Data. *J. Phys. Chem. B* **2006**, *110*, 17531−17538.

(50) Myers, A. L.; Monson, P. A. Adsorption in Porous Materials at High Pressure: Theory and Experiment. *Langmuir* **2002**, *18*, 10261−10273.

(51) Vuong, T.; Monson, P. A. Monte Carlo Simulation Studies of Heats of Adsorption in Heterogeneous Solids. *Langmuir* **1996**, *12*, 5425−5432.

(52) Nicholson, D. *Computer Simulation and the Statistical Mechanics of Adsorption*; Academic Press, 1982.

(53) Wang, W.; Peng, X.; Cao, D. Capture of Trace Sulfur Gases from Binary Mixtures by Single-Walled Carbon Nanotube Arrays: A Molecular Simulation Study. *Environ. Sci. Technol.* **2011**, *45*, 4832−4838.

(54) Rahimi, M.; Babu, D. J.; Singh, J. K.; Yang, Y.-B.; Schneider, J. J.; Muller-Plathe, F. Double-walled Carbon Nanotube Array for CO$_2$ and SO$_2$ Adsorption. *J. Chem. Phys.* **2015**, *143*, 169901

(55) Yi, H.; Wang, Z.; Liu, H.; Tang, X.; Ma, D.; Zhao, S.; Zhang, B.; Gao, F.; Zuo, Y. Adsorption of SO$_2$, NO, and CO$_2$ on Activated Carbons: Equilibrium and Thermodynamics. *J. Chem. Eng. Data* **2014**, *59*, 1556−1563.

(56) Grzyb, B.; Albiniak, A.; Broniek, E.; Furdin, G.; Mareche, J.; Begin, D. SO$_2$ Adsorptive Properties of Activated Carbons Prepared from Polyacrylonitrile and its Blends with Coal-tar Pitch. *Microporous Mesoporous Mater.* **2009**, *118*, 163−168.

(57) Molina-Sabio, M.; Munecas, A.; Rodriguez-Reinoso, F.; McEnaney, B. Adsorption of CO$_2$ and SO$_2$ on Activated Carbons with a Wide Range of Micropore Size Distribution. *Carbon* **1995**, *33*, 1777−1782.

(58) Dathe, H.; Peringer, E.; Roberts, V.; Jentys, A.; Lercher, J. A. Metal Organic Frameworks based on Cu2. and Benzene-1,3,5-Tricarboxylate as Host for SO$_2$ Trapping Agents. *C. R. Chim.* **2005**, *8*, 753−763.

(59) Tan, K.; Canepa, P.; Gong, Q.; Liu, J.; Johnson, D. H.; Dyevoich, A.; Thallapally, P. K.; Thonhauser, T.; Li, J.; Chabal, Y. J. Mechanism of Preferential Adsorption of SO$_2$ into Two Microporous Paddle Wheel Frameworks M(bdc)(ted)0.5. *Chem. Mater.* **2013**, *25*, 4653−4662.

(60) Song, X.-D.; Wang, S.; Hao, C.; Qiu, J.-S. Investigation of SO$_2$ Gas Adsorption in Metal-Organic Frameworks by Molecular Simulation. *Inorg. Chem. Commun.* **2014**, *46*, 277−281.

(61) Cui, X.; Yang, Q.; Yang, L.; Krishna, R.; Zhang, Z.; Bao, Z.; Wu, H.; Ren, Q.; Zhou, W.; Chen, B. et al. Ultrahigh and Selective SO$_2$ Uptake in Inorganic Anion-Pillared Hybrid Porous Materials. *Adv. Mater.* **2017**, *29*, 1606929.

(62) Yang, S.; Sun, J.; Ramirez-Cuesta, A. J.; Callear, S. K.; David, W. I. F.; Anderson, D. P.; Newby, R.; Blake, A. J.; Parker, J. E.; Tang, C. C.; et al. Selectivity and Direct Visualization of Carbon Dioxide and Sulfur Dioxide in a Decorated Porous Host. *Nat. Chem.* **2012**, *4*, 887.

(63) Savage, M.; Cheng, Y.; Easun, T. L.; Eyley, J. E.; Argent, S. P.; Warren, M. R.; Lewis, W.; Murray, C.; Tang, C. C.; Frogley, M. D.; et al. Selective Adsorption of Sulfur Dioxide in a Robust Metal-Organic Framework Material. *Adv. Mater.* **2016**, *28*, 8705−8711.

(64) Yang, S.; Liu, L.; Sun, J.; Thomas, K. M.; Davies, A. J.; George, M. W.; Blake, A. J.; Hill, A. H.; Fitch, A. N.; Tang, C. C.; et al. Irreversible Network Transformation in a Dynamic Porous Host Catalyzed by Sulfur Dioxide. *J. Am. Chem. Soc.* **2013**, *135*, 4954−4957.

(65) Campbell, J. A. le Châtelier's Principle, Temperature Effects, and Entropy. *J. Chem. Educ.* **1985**, *62*, 231.

(66) Zhi, Y.; Zhou, Y.; Su, W.; Sun, Y.; Zhou, L. Selective Adsorption of SO_2 from Flue Gas on Triethanolamine-Modified Large Pore SBA-15. *Ind. Eng. Chem. Res.* **2011**, *50*, 8698−8702.

(67) Liu, L.; Bhatia, S. K. Molecular Simulation of CO_2 Adsorption in the Presence of Water in Single-Walled Carbon Nanotubes. *J. Phys. Chem. C* **2013**, *117*, 13479−13491.

(68) Foo, K.; Hameed, B. Insights Into the Modeling of Adsorption Isotherm Systems. *Chem. Eng. J.* **2010**, *156*, 2−10.